

Supplementary Material

Modeling the Cholesteric Pitch of Apolar Cellulose Nanocrystal Suspensions Using a Chiral Hard-Bundle Model

Massimiliano Chiappini, Simone Dussi, Bruno Frka-Petescic,

Silvia Vignolini, Marjolein Dijkstra

(*Electronic mail: m.dijkstra@uu.nl)

(Dated: 8 December 2021)

THE MICROSCOPIC PITCH OF CNCS

The microscopic pitch length of CNCS is harder to extrapolate from a 2-dimensional electron microscope image. A precise experimental characterisation of the microscopic twist of CNCS is still lacking. The microscopic pitch was therefore estimated from all-atom Molecular Dynamics simulations of one single crystallite performed by Zhao *et al.*,² who showed that the axial twist (in degrees per nm) of cellulose microfibrils is shown to be linearly proportional to the inverse cross-sectional area, with a gradient of approximately 16 (deg/nm) per (1/nm²), see FIG. 6 of ref 2. Using a diameter of 6.3 nm for a single crystallite and approximating the crystallites as cylinders, we obtain a cross-section of about 31 nm², corresponding to an inverse cross-section of $\sim 1/31 \simeq 0.032 \text{ nm}^{-2}$. Extrapolating the data of ref 2 to this inverse cross-section gives an estimated twist of $16 * 0.032 \simeq 0.51 \text{ deg/nm}$, corresponding to a microscopic pitch length of approximately $360/0.51 \simeq 700 \text{ nm}$. However, this value is likely to overestimate the true crystallite cross-section. For that reason, we explore a range of microscopic pitch values from 375 up to 750 nm, demonstrating that the cholesteric pitch changes only mildly with the microscopic pitch (FIG. 4). We therefore choose a microscopic pitch of 500 nm as a typical value for further calculations.

The microscopic twist from ref 2 is right-handed along the twist axis \mathbf{t} . For relatively weak twisting distortions such as used in this work ($w \ll L \ll p$), the twisted ribbon nature of the CNC shape can be captured by the 3D coordinates of the four external corners of the ribbon. The twist introduced along \mathbf{t} has direct implications in the apparent twist with opposite handedness in the perpendicular direction. The microscopic pitch p causing a (right-handed) twisting rate $q_{\mathbf{t}} = +2\pi/p = 0.72 \text{ deg/nm}$ ($\approx +0.0126 \text{ rad/nm}$) in the \mathbf{t} axis implies an apparent (left-handed) twisting rate $q_{\perp\mathbf{t}} = -q_{\mathbf{t}} = -2\pi/p$ in the perpendicular direction. In the regime where $w \ll L \ll p$, a twist along \mathbf{t} is almost indistinguishable from a twist perpendicular to \mathbf{t} . The validity of this

work is thus not expected to be affected by the definition of the twist axis used here.

EFFECT OF BIDISPERSITY IN (L,w) ON THE PITCH \mathcal{P}

In FIG. S1-S2, we plot the macroscopic pitch length \mathcal{P} as a function of the effective w/w mass fraction of the cholesteric phase of a bidisperse suspension of chiral hard splinters for varying volume ratios $\phi_{(+)}$ and sizes ($L_{(\pm)} = L(1 \pm \delta)$ and $w_{(\pm)} = w(1 \pm \delta)$) defined by $\delta = 0.0, 0.1, 0.2, 0.3$ and 0.4 as obtained from DFT calculations.

CHARACTERISTICS OF THE CNC SHAPE

In this work, the length L is defined tip-to-tip and includes the spherocylinder cap diameter (excluding the surfactant layer), so that the length definition coincides with the definition of experimental CNC dimensions. The width w is the outer dimension (without the surfactant layer) and also includes the spherocylinder diameter, to satisfy the same definition.

We calculate the effective density of CNCs with adsorbed surfactants as $\rho_{\text{eff}} = \rho_S \phi_S + \rho_{\text{CNC}} (1 - \phi_S)$, where $\rho_S = 1120 \text{ kg.m}^{-3}$ denotes the density of the BNA surfactants and $\rho_{\text{CNC}} = 1600 \text{ kg.m}^{-3}$ the density of the bare CNCs. We then calculate the effective w/w mass fraction from the packing fraction η as $c_{\text{eff}} = \rho_{\text{eff}} \eta / (\rho_{\text{eff}} \eta + \rho_{\text{solv}} (1 - \eta))$, where $\rho_{\text{solv}} = 779 \text{ kg.m}^{-3}$ is the density of the solvent cyclohexane. Table S1 summarizes the dimension characteristics of the bundles and how their mass fraction is derived for the case of BNA in cyclohexane. In this table, $v_0(0)$ is the volume of bare CNCs, $v_0(\lambda_S)$ is the volume of the CNCs with a surfactant layer of thickness λ_S , ϕ_S is the volume ratio of surfactants ($= [v_0(\lambda_S) - v_0(0)] / v_0(\lambda_S)$), m_{CNC} is the mass of bare CNCs and m_S is mass of surfactants.

In a bidisperse suspension of two populations $\{(+), (-)\}$ of CNCs, the total mass fraction c_{eff}

is obtained by first determining the volumic mass of each subpopulation:

$$\rho_{\text{eff},(+)} = \rho_S \phi_{S,(+)} + \rho_{\text{CNC},(+)}(1 - \phi_{S,(+)}) \quad (1)$$

$$\rho_{\text{eff},(-)} = \rho_S \phi_{S,(-)} + \rho_{\text{CNC},(-)}(1 - \phi_{S,(-)}), \quad (2)$$

where $\phi_{S,(\pm)}$ denotes the volume ratio of surfactants for a single large (small) CNC, and $\rho_{\text{eff},(\pm)}$ the effective mass density of large (small) CNCs with adsorbed surfactants. The volume fraction of each subpopulation is defined as:

$$\eta_{(+)} = \frac{x_{(+)}v_{(+)}}{x_{(+)}v_{(+)} + x_{(-)}v_{(-)}} \eta \quad ; \quad \eta_{(-)} = \frac{x_{(-)}v_{(-)}}{x_{(+)}v_{(+)} + x_{(-)}v_{(-)}} \eta \quad (3)$$

where $v_{(\pm)}$ denotes the volume of a single large (small) CNC including the surfactant layer, and η is the total packing fraction. The final mass fraction c_{eff} is then expressed as:

$$c_{\text{eff}} = \frac{\rho_{\text{eff},(+)}\eta_{(+)} + \rho_{\text{eff},(-)}\eta_{(-)}}{\rho_{\text{eff},(+)}\eta_{(+)} + \rho_{\text{eff},(-)}\eta_{(-)} + \rho_S(1 - \eta_{(+)} - \eta_{(-)})} \quad (4)$$

For comparison, the pitch lengths reported as a function of the effective w/w mass fraction c_{eff} in the main text are reported here as a function of the packing fraction η in FIG. S6 and S8-S11.

RESEARCH DATASET IN OPEN ACCESS

Additional data related to this publication is available at the University of Cambridge data repository (<https://doi.org/10.17863/CAM.53675>).

REFERENCES

- ¹C. Honorato-Rios, J. P. F. Lagerwall, *Communications Materials* **1**, 69 (2020).
²Z. Zhao, O.E. Shklyaev, A. Nili, M.N.A. Mohamed, J.D. Kubicki, V.H. Crespi, and L. Zhong, *The Journal of Physical Chemistry A* **117**, 2580 (2013).

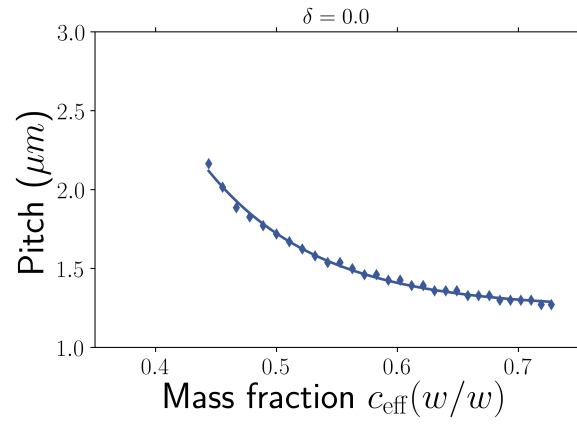


FIG. S1: The macroscopic pitch length \mathcal{P} as a function of the effective w/w mass fraction of the cholesteric phase of a monodisperse suspension of chiral hard splinters ($\delta = 0$), as obtained from DFT calculations. This is the reference shown in FIG. S2-S3.

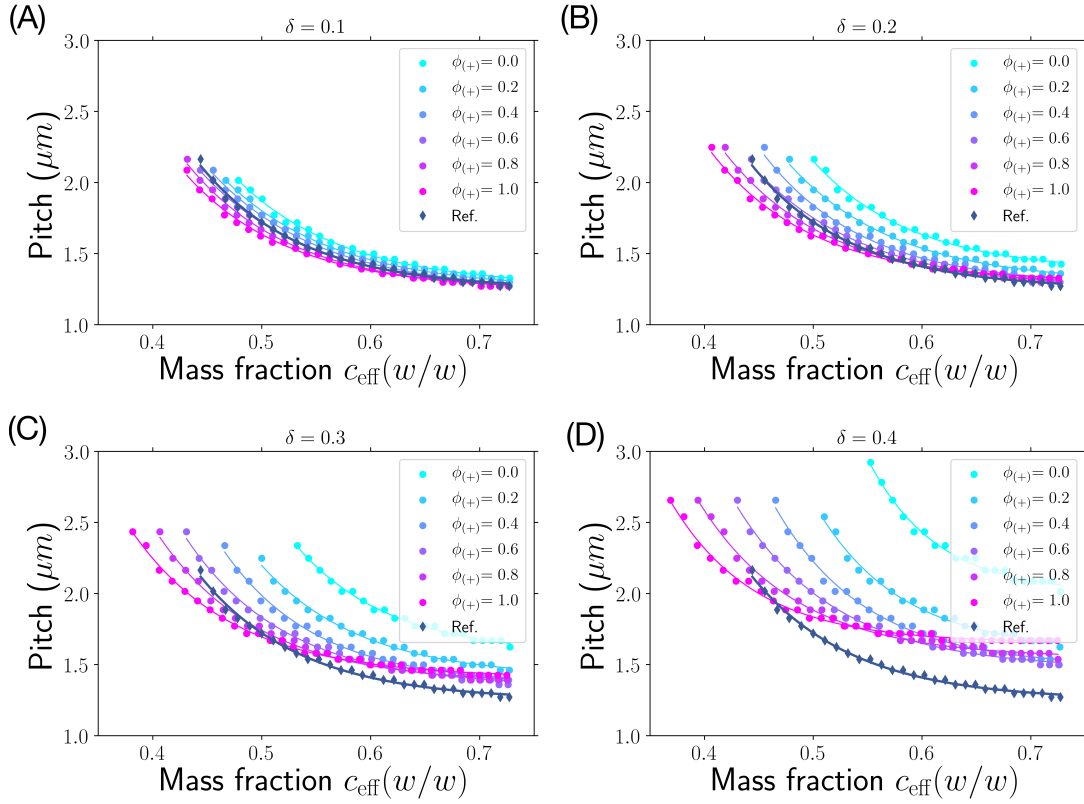


FIG. S2: The macroscopic pitch length \mathcal{P} as a function of the effective w/w mass fraction of the cholesteric phase of a bidisperse suspension of chiral hard splinters for varying volume ratios $\phi_{(+)}$ and sizes $L_{(\pm)} = L(1 \pm \delta)$ and $w_{(\pm)} = w(1 \pm \delta)$ defined by A) $\delta = 0.1$ and B) $\delta = 0.2$, C) $\delta = 0.3$, D) $\delta = 0.4$, as obtained from DFT calculations. The monodisperse case ($\delta = 0$ and labeled Ref.) is displayed for reference.

TABLE S1: Dimensions of the bundles used to model the different CNC shapes.

δ [\emptyset]	Label	L [nm]	$L+2\lambda_S$ [nm]	w [nm]	$w+2\lambda_S$ [nm]	$v_0(0)$ [10^3 nm^3]	$v_0(\lambda_S)$ [10^3 nm^3]	ϕ_S [\emptyset]	m_{CNC} [10^{-20} kg]	m_S [10^{-20} kg]
-40%	(L-)	76.80	79.80	26.00	29.00	9.29	17.52	0.47	1.49	2.41
	(w-)	128.0	131.00	15.60	18.60	9.89	17.85	0.45	1.58	2.47
	(-)	76.80	79.80	15.60	18.60	6.32	11.44	0.45	1.01	1.58
-30%	(L-)	90.00	93.00	26.00	29.00	10.83	20.14	0.46	1.73	2.78
	(w-)	128.00	131.00	18.20	21.20	11.39	20.26	0.44	1.82	2.82
	(-)	90.00	93.00	18.20	21.20	8.43	15.06	0.44	1.35	2.09
-20%	(L-)	102.40	105.40	26.00	29.00	12.27	22.64	0.46	1.96	3.12
	(w-)	128.00	131.00	20.80	23.80	12.76	22.63	0.44	2.04	3.15
	(-)	102.40	105.40	20.80	23.80	10.62	18.92	0.44	1.70	2.63
-10%	(L-)	115.20	118.20	26.00	29.00	13.64	24.92	0.45	2.18	3.45
	(w-)	128.00	131.00	23.40	26.40	13.96	24.95	0.44	2.23	3.46
	(-)	115.20	118.20	23.40	26.40	12.81	22.97	0.44	2.05	3.19
0%	Ref.	128.00	131.00	26.00	29.00	14.91	27.08	0.45	2.39	3.75
+10%	(L+)	140.80	143.80	26.00	29.00	16.06	29.00	0.45	2.57	4.02
	(w+)	128.00	131.00	28.60	31.60	15.48	29.06	0.47	2.48	4.00
	(+)	140.80	143.80	28.60	31.60	16.77	31.13	0.46	2.68	4.29
+20%	(L+)	153.60	156.60	26.00	29.00	17.06	30.77	0.45	2.73	4.27
	(w+)	128.00	131.00	31.20	34.20	15.75	30.83	0.49	2.52	4.21
	(+)	153.60	156.60	31.20	34.20	18.47	35.07	0.47	2.96	4.81
+30%	(L+)	166.40	169.40	26.00	29.00	17.96	32.30	0.44	2.87	4.48
	(w+)	128.00	131.00	33.80	36.80	15.78	32.34	0.51	2.52	4.38
	(+)	166.40	169.40	33.80	36.80	20.05	38.76	0.48	3.21	5.30
+40%	(L+)	179.20	182.20	26.00	29.00	18.74	33.60	0.44	3.00	4.66
	(w+)	128.00	131.00	36.40	39.40	15.82	33.59	0.53	2.53	4.52
	(+)	179.20	182.20	36.40	39.40	21.54	42.16	0.49	3.45	5.76

TABLE S2: Conversion between number fraction $x_{(+)}$ and volume ratio $\phi_{(+)}$ of the large CNCs for the bidisperse case.

$\delta = 0.1$		$\delta = 0.2$		$\delta = 0.3$		$\delta = 0.4$	
$x_{(+)}$	$\phi_{(+)}$	$x_{(+)}$	$\phi_{(+)}$	$x_{(+)}$	$\phi_{(+)}$	$x_{(+)}$	$\phi_{(+)}$
0.00	0.000	0.00	0.000	0.00	0.000	0.00	0.000
0.20	0.253	0.20	0.317	0.20	0.392	0.20	0.479
0.40	0.475	0.40	0.553	0.40	0.632	0.40	0.710
0.60	0.670	0.60	0.735	0.60	0.795	0.60	0.847
0.80	0.844	0.80	0.881	0.80	0.912	0.80	0.936
1.00	1.000	1.00	1.000	1.00	1.000	1.00	1.000

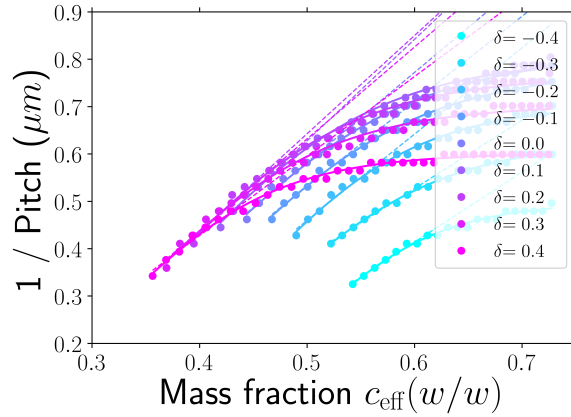


FIG. S3: Inverse of the macroscopic pitch length, $1/\mathcal{P}$, as a function of the scaling parameter δ impacting both the length L and the width w in a monodisperse suspension. A linear fit $1/\mathcal{P} = A(c_{\text{eff}} - c_0)$, is extracted from the first 8 data points at low mass fraction.

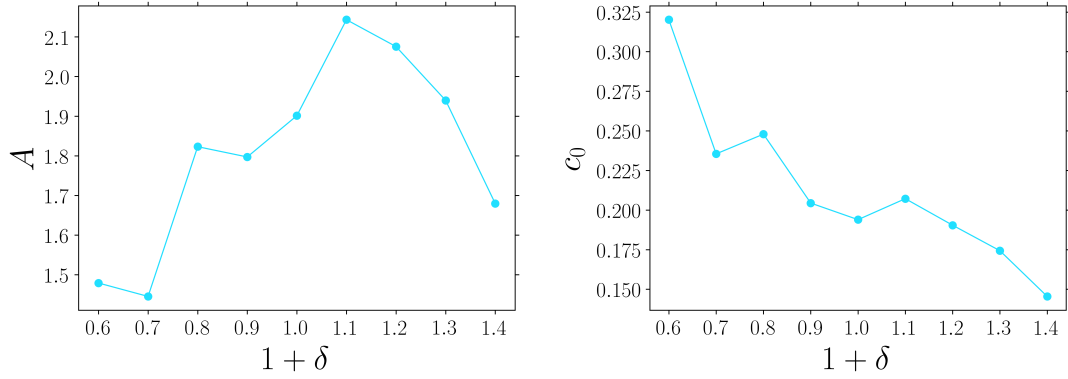


FIG. S4: Variation with the scaling factor δ of the extracted parameters A and c_0 , as from the linear extrapolation of $1/\mathcal{P}$ vs. c_{eff} at low mass fraction.

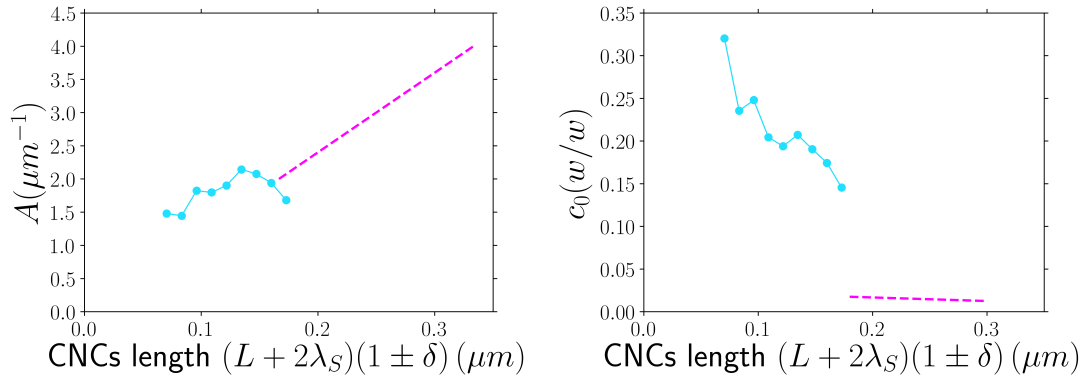


FIG. S5: Same extracted parameters A and c_0 as in FIG. S4, vs. the CNC length $(L + 2\lambda_S)(1 + \delta)$, allowing for a comparison with data from ref.¹.

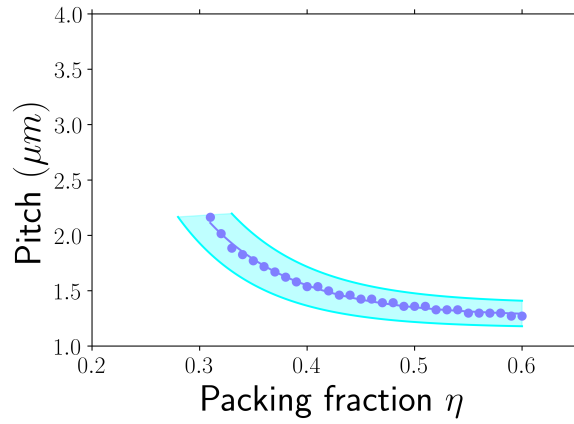


FIG. S6: Macroscopic pitch length \mathcal{P} obtained from DFT calculations from FIG. 3 and FIG. S1, reported as a function of the packing fraction η .

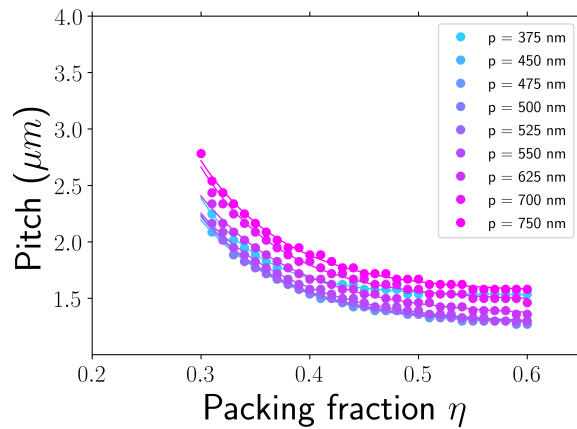


FIG. S7: Macroscopic pitch length \mathcal{P} obtained from DFT calculations for varying values of the microscopic pitch p of the bundles from FIG. 4, reported as a function of the packing fraction η .

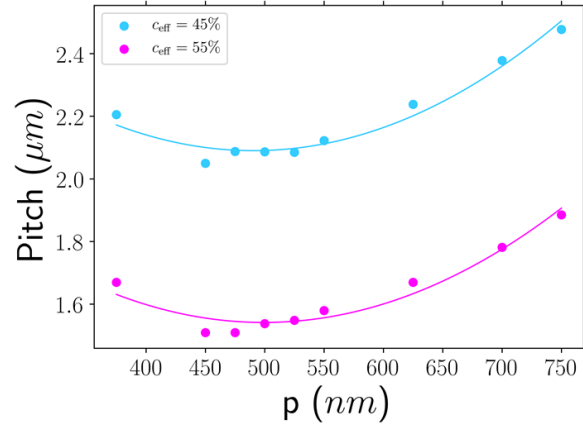


FIG. S8: Macroscopic pitch length \mathcal{P} obtained from DFT calculations for two mass fractions $c_{\text{eff}} = 45\%$ and $c_{\text{eff}} = 55\%$, reported as a function of the microscopic pitch p .

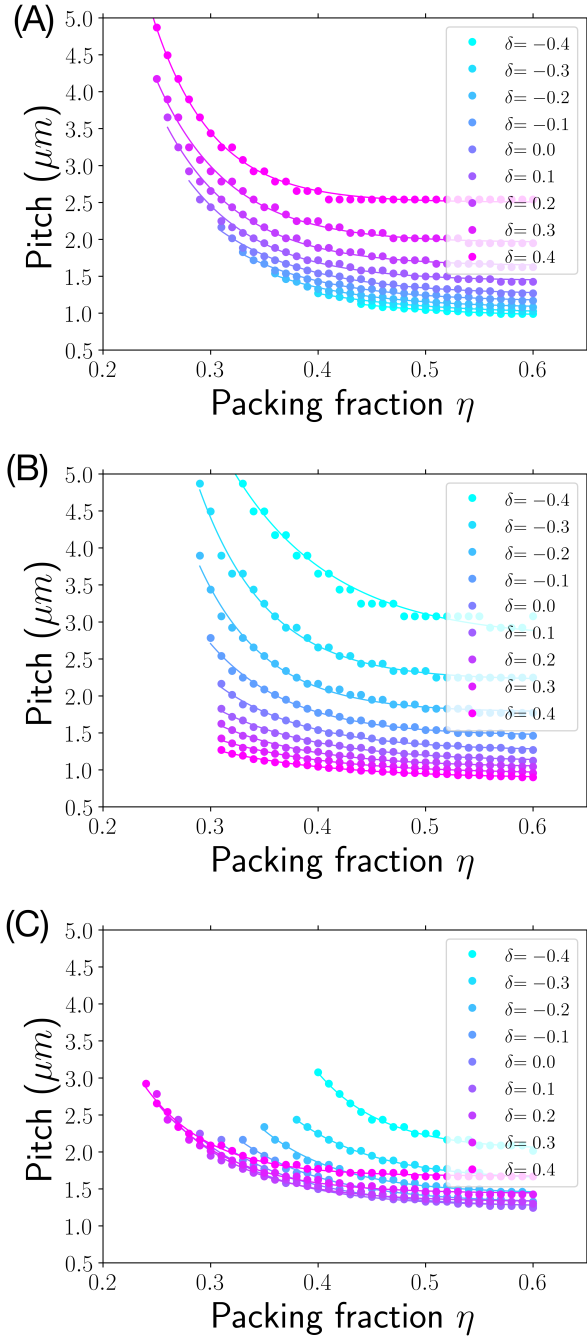


FIG. S9: Macroscopic pitch length \mathcal{P} obtained from DFT for a cholesteric phase of monodisperse chiral hard-splinters of different (A) length, (B) width, and both length and width (C) from FIG. 5, reported as a function of the packing fraction η .

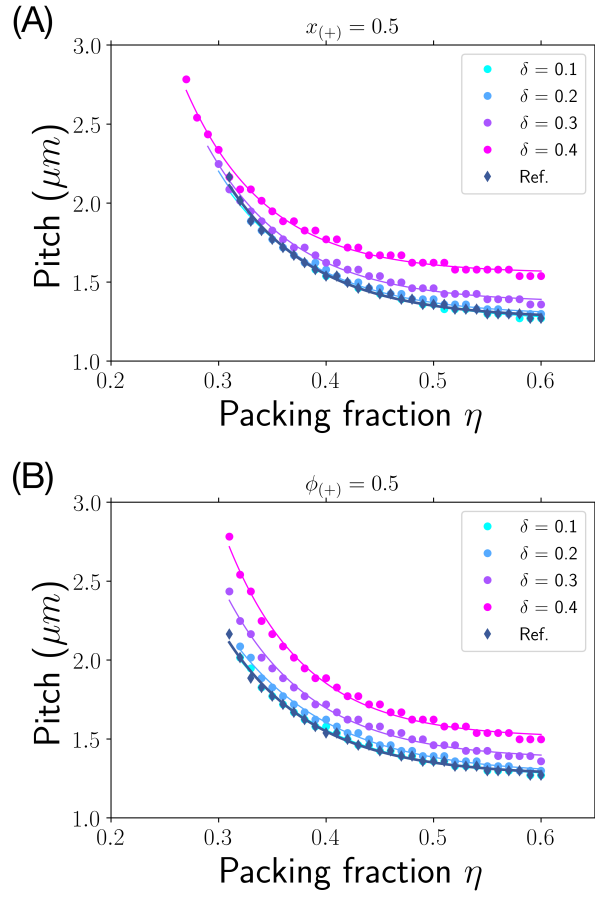


FIG. S10: Macroscopic pitch length \mathcal{P} obtained from DFT for a cholesteric phase of bidisperse chiral hard-splinters of various sizes and fixed L/w aspect ratio at (A) equal number fraction ($x_{(+)} = x_{(-)} = 1/2$) or (B) equal volume ratio ($\phi_{(+)} = \phi_{(-)} = 1/2$) from FIG. 6, reported as a function of the packing fraction η .

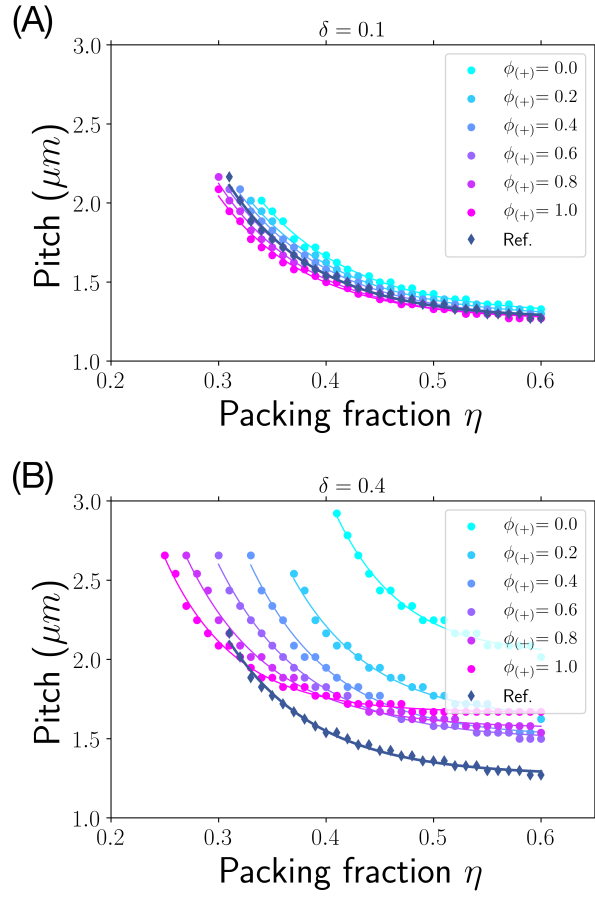


FIG. S11: Macroscopic pitch length \mathcal{P} obtained from DFT for a cholesteric phase of bidisperse chiral hard-splinters of large and small particles of fixed L/w aspect ratio and various volume ratios $\phi_{(+)}$ of large particles for (A) $\delta = 0.1$ and (B) $\delta = 0.4$ from FIG. 7, reported as a function of the packing fraction η